The ultrafast energy transfer process in naphtole–nitrobenzofurazan bichromophoric molecular systems. A study by femtosecond UV–vis pump–probe spectroscopy

ARTICLE · APRIL 2007

DOI: 10.1016/j.jphotochem.2006.10.020

9 AUTHORS, INCLUDING:

Pier Luigi Gentili
Università degli Studi di Perugia
56 PUBLICATIONS **782** CITATIONS
SEE PROFILE

Roberto Righini
University of Florence
171 PUBLICATIONS **4,041** CITATIONS
SEE PROFILE

Paolo Foggi
Università degli Studi di Perugia
119 PUBLICATIONS **1,641** CITATIONS
SEE PROFILE

Alberto Brandi
University of Florence
289 PUBLICATIONS **4,684** CITATIONS
SEE PROFILE

Available online at www.sciencedirect.com
ScienceDirect
Journal of Photochemistry and Photobiology A: Chemistry 187 (2007) 209–221
Journal of Photochemistry and Photobiology A:Chemistry
www.elsevier.com/locate/jphotochem

The ultrafast energy transfer process in naphtole–nitrobenzofurazan bichromophoric molecular systems
A study by femtosecond UV–vis pump-probe spectroscopy

Pier Luigi Gentili [a,1], Martina Mugnai [a,2], Laura Bussotti [a], Roberto Righini [a,2], Paolo Foggi [a,*,1], Stefano Cicchi [b,**], Giacomo Ghini [b], Simone Viviani [b], Alberto Brandi [b]

[a] *LENS, via Nello Carrara 1, Polo Scientifico Universitario, Sesto F.no. (FI), Italy*
[b] *Department of Organic Chemistry, Polo Scientifico Universitario, Sesto F.no. (FI), Italy*

Received 6 July 2006; received in revised form 25 September 2006; accepted 9 October 2006
Available online 10 November 2006

Abstract

This work presents an experimental and computational study of the intramolecular electronic energy transfer process occurring in two newly synthesized bichromophoric species: *N-(7-nitro-2,1,3-benzoxadiazol-4-yl)amino-bis-ethyl-2-[(4-chloro-1-naphthyl)oxy]acetate* (***f-Bi***) and *N-(7-nitrobenzo[c][1,2,5]oxadiazole-4-yl)-(3S, 4S)-pyrrolidin-3,4-bis-yl-2-[(4-chloro-1-naphthyl)oxy]acetate* (***r-Bi***). In both ***f-Bi*** and ***r-Bi*** the donor chromophore is the *[(4-chloro-1-naphthyl)oxy]acetate* moiety, whereas the acceptor units belong to the family of the 4-dialkylaminonitrobenzoxadiazoles, well-known fluorescent probes. The two bichromophores differ in the structural flexibility. In ***f-Bi***, acceptor and donors are linked by a diethanolamine moiety, whereas in ***r-Bi*** through a (3S, 4S)3,4-dihydroxypyrrolidine ring. By means of steady-state and time-resolved UV–vis spectroscopies we carried out a detailed analysis of the photo-response of donor and acceptor chromophores as individual molecules and when covalently linked in ***f-Bi*** and ***r-Bi***. The intramolecular energy transfer process occurs very efficiently in both the bichromophores. The rate constant and the quantum efficiency of the process are $k_{ET} = (2.86 \pm 0.16) \times 10^{11}\ s^{-1}$ and $Q = 0.998$ in ***f-Bi***, and $k_{ET} = (1.25 \pm 0.08) \times 10^{11}\ s^{-1}$ and $Q = 0.996$ in ***r-Bi***. Semiempirical calculations were utilized to identify the energy and the nature of the electronic states in the isolated chromophores. Molecular mechanics calculations have been performed to identify the most stable structures of the bichromophoric compounds. The predictions of Förster theory are consistent with the experimental results and provide a suitable way to evaluate the structural differences between the two compounds.

Keywords: Electronic energy transfer; Bichromophores; Ultrafast spectroscopy; Transient absorption

1. Introduction

The process of electronic energy transfer (EET) is ubiquitous in natural and artificial photochemically active systems [1,2]. It is present in the antenna systems of photosynthetic organisms [2–6], in photodynamic therapy [7,8], in multichromophoric β-cyclodextrins [9,10], in photomolecular devices [11–14] and in photochemical synthesis [15]. It occurs in systems composed of at least two molecular species [1,16,17]: a donor (Dn) and an acceptor (Ac). EET processes take place at distances from 1 Å to more than 50 Å, and on time scales ranging from femtoseconds to milliseconds [16,17]. When Dn and Ac are parts of the same compound, the EET is intramolecular (intra-EET), otherwise the EET is intermolecular (inter-EET).

Inter-EET and intra-EET are special cases of non-radiative processes contributing to the decay of electronically excited molecular systems [18–22]. Depending on the relative magnitude of the electronic coupling between donor and acceptor (V_{Dn-Ac}) and on the donor vibronic bandwidth, two limiting cases of EET can be distinguished, which are referred to as

* Corresponding author. Tel.: +39 0554572494; fax: +39 0554572521.
** Corresponding author. Tel.: +39 0554573496; fax: +39 0554573531.
E-mail addresses: FOGGI@LENS.UNIFI.IT (P. Foggi), STEFANO.CICCHI@UNIFI.IT (S. Cicchi).
[1] Department of Chemistry, University of Perugia, Italy.
[2] Department of Chemistry, Polo Scientifico Universitario, Sesto F.no. (FI), Italy.

1010-6030/$ – see front matter © 2006 Elsevier B.V. All rights reserved.
doi:10.1016/j.jphotochem.2006.10.020

strong and weak coupling mechanisms, respectively [1,23]. In the strong coupling case the excitation is delocalized on both the donor and the acceptor. Within the weak-coupling regime, the rate for energy transfer k_{ET} between an excited donor and a ground-state acceptor can be derived from the time-dependent perturbation theory and the Fermi Golden Rule as [1]

$$k_{ET} = \frac{2\pi}{\hbar}|V_{Dn-Ac}|^2(FCWD) \quad (1)$$

where FCWD represents the *Frank-Condon weighted density* of states, corresponding to the product of the density of vibrational states in the initial and final states and their spectral overlap. In general, the effective electronic coupling matrix element V_{Dn-Ac} can be expressed as a sum of a number of electronic coupling terms [1,24]:

$$V_{Dn-Ac} = u^{Coulombic} + u^{short\text{-}range} + u^{bridge} \quad (2)$$

where $u^{Coulombic}$ represents through-space acting Coulombic interaction between dipoles and/or higher multipoles; $u^{short\text{-}range}$ is the Dexter type mechanism, depends upon the interchromophore orbital overlap, consists of a term accounting for the interpenetration of the charge density centered on one molecule with that of the other molecule and of an exchange term defining the quantum mechanical two-electron exchange interaction; u^{bridge} accounts for the transfer of energy from the donor to the acceptor via intermediate moieties or connecting bridges [1,24].

Understanding the mechanism of EET between two chromophores is the key for the design and construction of efficient photonic devices, artificial energy harvesting systems, and it is of interest in optical computing and in molecular electronics [25,26].

Bichromophoric molecules, containing two or more distinguishable molecular units separated by bridges of controllable length, are ideal systems for investigating intra-EET processes [17]. The properties of the bridge determine the degree of flexibility of the whole structure and the basic electronic structure of the chromophores. If the bridge prevents the direct Dn–Ac interaction, the electronic absorption spectrum of the bichromophore can be described as a simple superposition of the absorption spectra of the two chromophores. On the other hand, if the bridge induces reciprocal interaction of the two chromophores, the optical properties of the bichromophoric species result "non-additive" [1,2,27].

In this paper we present the study of the intra-EET process in two newly synthesized bichromophoric species where the *(4-chloro-naphthalen-1-yloxy)-acetyl* group acts as the donor and the *N-(7-nitro-2,1,3-benzoxadiazol-4-yl)bis-ethanolamine* and *N-(7-nitrobenzo[c][1,2,5]oxadiazole-4-yl)-(3S, 4S)-pyrrolidine-3,4-diol* act as acceptors (see Plate 1). The two moieties are covalently linked through an ester functionality.

4-dialkylaminonitrobenzoxadiazoles are frequently utilized fluorescent probes in biological applications [28–31]. The presence at the opposite ends of an aromatic ring system of electron-donating and -accepting groups, such as amino- and nitro-groups, produces fluorophores particularly sensitive to their surroundings [32]. In addition, the two Ac units, bridged with the flexible di-ethanolamine and the rigid 3,4-diol-pyrrolidine groups, respectively, offer an excellent opportunity for investigating the dependence of intra-EET on molecular flexibility. The Dn chromophore has been chosen in order to maximise the efficiency of the EET process. In fact, the emission band of the *(4-chloro-naphthalen-1-yloxy)-acetyl* donor largely coincides with the S_2 state absorption band of Ac.

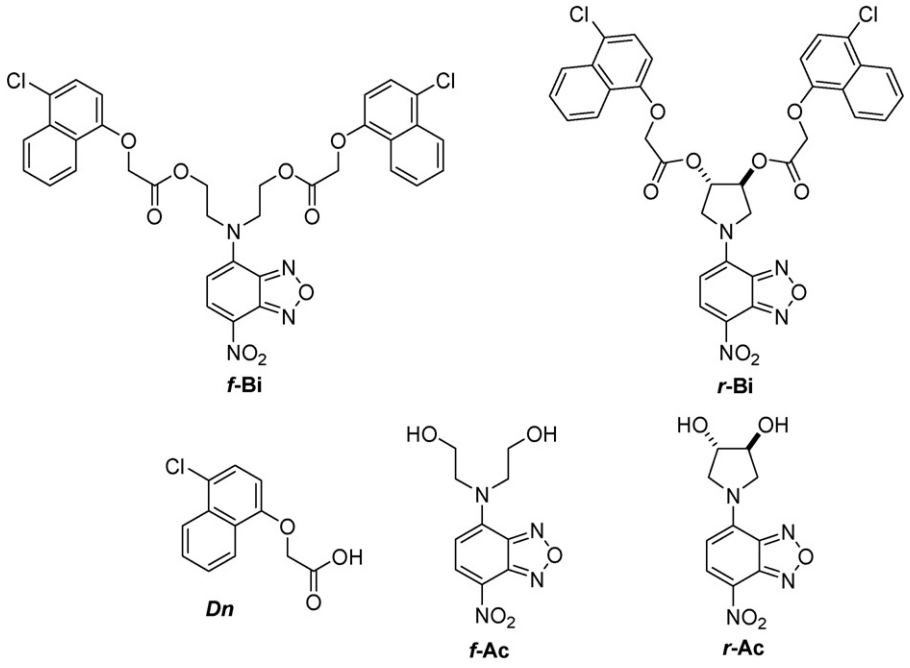

Plate 1. The molecular structure of the two bichromophores, the two acceptors and the donor.

2. Experimental and data handling

2.1. Materials and synthesis of the compounds

All materials for the synthesis of Ac, Dn and of the two bichromophores were purchased from Aldrich. The solvents for the spectroscopic measurements, acetonitrile (≥99.9%) from Merck and ethanol (∼96%) from Fluka were used as received.

The donor Dn, (4-chloro-naphthalen-1-yloxy)-acetic acid, was synthesized according to the procedure reported in Ref. [33].

2.1.1. 4-(diethanolamino)-7-nitro-benzo [1,2,5]oxadiazole (f-Ac)

A solution of 4-chloro-7-nitro-benzofurazane (2.1 mmol, 420 mg) with diethanol-ammine (3 mmol, 320 mg, 300 μl) in 10 ml ethyl-acetate and 1 ml dichloro-methane, was left under vigorous stirring at room temperature (rt). After 2 h the dark red solution was added with triethyl-amine (1.2 mmol, 110 mg, 140 μl) and kept under stirring for 2 h. Finally the solution was concentrated and the red dark solid was recristallyzed from methanol/diethyl ether to give 540 mg of a red solid (95% yield). R_f (CH_2Cl_2/MeOH 4:1) = 0.8; mp 194–196 °C; ^{1}H NMR (200 MHz, $CDCl_3$/CD_3OD): δ 8.45 (d, J = 9 Hz, 1H), 6.41 (d, J = 9 Hz, 1H), 4.20 (t, J = 5 Hz, 4H), 3.95 (t, J = 5 Hz, 4H). ^{13}C NMR (50 MHz, $CDCl_3$/CD_3OD): δ 145.6, 144.1, 144.0, 135.3, 120.5, 101.9, 58.3, 55.7; MS EI 70 eV *m/z* 268.1 (M^+, 20.5), 269.3 (2), 270.3 (0.4); IR KBr: 3366 (m, b), 3111 (w), 2953 (w), 2937 (w), 2884 (w), 1606 (s), 1552 (s, b), 1483 (m), 1458 (m), 1450 (m), 1431 (m), 1388 (m), 1328 (s), 1300 (s), 1252 (m), 1225 (m), 1163 (m), 1061 (s), 1003 (m) cm^{-1}; Anal. Calcd for $C_{10}H_{12}N_4O_5$C, 44.78; H, 4.51; N, 20.89; Found C, 44.75; H, 4.24; N, 21.00.

2.1.2. N-(7-nitro-2,1,3-benzoxadiazol-4-yl)amino-bis-ethyl-2-[(4-chloro-1-naphthyl)oxy]acetate (f-Bi)

A solution of 4-chloro-naphthalen-1-yloxy-acetic acid (1 equiv., 0.71 mmol, 170 mg) in 6 ml dry dichloro-methane and 0.1 ml DMF, was added with oxalyl chloride (1.1 equiv., 0.8 mmol, 99 mg, 66 μl,) as reported in Ref. [34]. f-Ac (1 equiv., 0.36 mmol, 97 mg) was added slowly at 0 °C to the resulting solution followed by the addition of pyridine (3 equiv., 2.4 mmol, 193 μl). The dark red solution was stirred at rt overnight and concentrated to produce the crude reaction mixture which was purified by column chromatography to give 80 mg (yield 36%) of (f-Bi). R_f(CH_2Cl_2) = 0.45; mp 75–76 °C). ^{1}H NMR (400 MHz, DMSO): δ 8.25 (d, J = 9 Hz, 1H), 8.13–8.20 (m, 2H), 8.06–8.05 (m, 2H), 7.70–7.66 (m, 2H), 7.60–7.56 (m, 2H), 7.46 (d, J = 8 Hz, 2H), 6.80 (d, J = 8 Hz, 2H), 6.48 (d, J = 9 Hz, 1H), 4.96 (s, 1H), 4.47 (t, J = 5 Hz, 4H), 4.20 (m, 4H); ^{13}C NMR (50 MHz, $CDCl_3$): δ 168.2, 152.1, 144.0, 143.9, 143.7, 134.4, 131.1, 127.8, 126.3, 126.0, 125.1, 124.3, 124.1, 123.4, 122.0, 104.5, 101.8, 65.3, 62.2, 51.6; MS EI 70 eV *m/z* 705.5 (M^+, 0.9); IR KBr: 3435 (m), 3.066(w), 2962(w), 2924(w), 1762(s), 1742(s), 1614(m), 1593(m), 1544 (s), 1383 (s), 1301(s), 1278(s), 1195(s), 1097(s) cm^{-1}; Anal. Calcd for $C_{34}H_{26}Cl_2N_4O_9$ C, 57.88; H, 3.71; N, 7.94; Found C, 57.87; H, 3.91; N, 7.99.

2.1.3. (3S, 4S)N-(7-nitrobenzo[c][1,2,5]oxadiazol-4-yl)-pyrrolidine-3,4-diol (r-Ac)

A solution of (3S, 4S)-*N*-benzyl 3,4-dihydroxypyrrolidine (1.1 mmol, 215 mg) in MeOH (5 ml) was added with $Pd(OH)_2$/C (110 mg) and left under an H_2 atmosphere with magnetic stirring overnight. The solution was then filtered and added with 4-Chloro-7-nitro-benzofurazane (1.6 mmol, 320 mg). After stirring for 3 h at rt a red solid precipitated. The suspension was filtered to give 255 mg of (*r-Ac*) (85% yield). $[\alpha]_D^{28}$ = −39.8 (C = 1, CH_2Cl_2).^{1}H NMR (200 MHz, $CDCl_3$/CD_3OD): δ 8.51 (d, J = 9 Hz, 1H), 6.21 (d, J = 9 Hz, 1H), 4.49–4.21 (m, 4H), 4.05 (m, 1H), 3.76–3.52 (m, 1H); ^{13}C NMR (50 MHz, $CDCl_3$/CD_3OD): δ 146.2, 144.1, 143.9, 135.2, 119.8, 100.5, 73.8, 72.6, 57.9, 55.3; MS EI 30 eV *m/z* 266 (M^+, 65); IR KBr: 3399 (s,b), 3285 (m), 3095 (w), 3078 (w), 3043 (w), 2930 (w), 2845 (w), 1609 (s), 1556 (s), 1535 (m), 1474 (m), 1425 (m), 1319 (s), 1276 (s), 1160 (m), 1077 (m), 1001 (m), 916 (m) cm^{-1}; Anal. Calcd for $C_{10}H_{10}N_4O_5$ C, 45.12; H, 3.79; N, 21.05; Found C, 45.19; H, 3.96; N, 21.04.

2.1.4. N-(7-nitrobenzo[c][1,2,5]oxadiazole-4-yl)-(3S,4S)-pyrrolidin-3,4-bis-yl2-[(4-chloro-1-naphthyl)oxy]acetate (r-Bi)

r-Ac (1.29 mmol, 344 mg) was added to the solution of (4-chloro-naphthalen-1-yloxy)-acetyl chloride (compare synthesis of *f-Bi*). The mixture was stirred overnight and then concentrated and purified by column chromatography to produce 270 mg of *r-Bi* (30% yield), R*f* (CH_2Cl_2) = 0.5, $[\alpha]_D^{28}$ = −39.8 (c = 1.00, CH_2Cl_2); ^{1}H NMR (400 MHz, CD_3CN): δ 8.38 (d, J = 9 Hz, 1H), 8.21–8.20 (m, 2H), 7.95–7.72 (m, 2H), 7.51–7.39 (m, 4H), 7.39–7.28 (m, 2H), 6.75 (d, J = 8 Hz, 2H), 5.63 (d, J = 9 Hz, 1H), 5.44-5.42 (m, 2H), 5.01–4.90 (m, 4H), 4.02–3.87 (m, 1H), 3.71–3.60 (m, 1H) 3.40–3.20 (m, 2H); ^{13}C NMR (DMSO, 50 MHz): δ 168.4, 152.7, 145.3, 145.2, 137.4, 136.1, 131.3, 129.0, 127.6, 126.9, 124.7, 124.5, 124.1, 123.6, 123.1, 122.1, 107.6, 103.5, 75.1, 74.0, 65.3, 56.6, 54.5; MS EI 30 eV *m/z* 703.8 (M^+, 100); IR KBr: 3507 (w, b), 3085 (w), 2919 (w), 2868 (w), 1766 (s), 1615 (m), 1592 (m), 1556 (s), 1505 (M), 1457 (M), 1423 (M), 1380 (M), 1316 (S), 1277 (S), 1189 (S), 1103 (S), 1000 (M) cm^{-1}; Anal. Calcd for $C_{34}H_{24}Cl_2N_4O_9$ C, 58.05; H, 3.44; N, 7.96; Found C, 58.41; H, 3.51; N, 7.73.

2.2. Spectroscopic measurements

UV–vis absorption measurements were performed on a Perkin-Elmer Lambda 5 spectrometer. Corrected fluorescence emission and excitation spectra were recorded on a Perkin-Elmer LS50B spectrofluorimeter. For fluorescence quantum yield (Φ_F) measurements, the absorbances at the excitation wavelengths were kept below 0.1. Anthracene in ethanol (Φ_F = 0.27) [35] and Fluorescein in 0.1 M NaOH (Φ_F = 0.93) [36] were used as standards.

The experimental instrumentation and the data processing for femtosecond transient absorption spectroscopy (TAS) have been described in detail in previous papers [37–39]. Ultrashort pulses (duration ∼100 fs at 800 nm, repetition rate = 1 kHz,

energy = 700 μJ/pulse) were produced by a regenerative amplified Ti:sapphire laser system. Tunable excitation pulses were obtained by means of a BBO-based optical parametric generator and amplifier (OPG-OPA). The direct excitation of the molecular *f-Ac* and *r-Ac* was achieved by tuning the pump pulse at 355 and 480 nm; these frequencies were obtained as the fourth harmonic of the OPG-OPA signal at 1.42 μm and as the sum frequency of the fundamental (800 nm) with the signal (1.20 μm), respectively (average power ∼2 mW). Dn and the two bichromophores were excited at 305 nm (fourth harmonic of the signal at 1.22 μm). A small portion (2 μJ/pulse) of the 800 nm beam was focused on a 2 mm thick CaF_2 plate to generate a pulse of white-light continuum. This latter spanned the entire visible region and extended into the near UV down to 350 nm. The white-light continuum was further split into two parts of equal intensity. One part, acting as a probe beam, was spatially overlapped with the excitation beam in the sample. The second part crossed the sample in a different position and provided the reference beam. The probe and reference beams were spectrally dispersed in a flat-field 25 cm Czerny-Turner spectrometer, and detected by means of a back-illuminated CCD camera with spectral response in the region 300–1000 nm. In all the experiments the relative pump-probe polarization was kept at 54.7° to discriminate the excited state against the orientational dynamics [37].

For kinetics measurements the probe wavelength was properly selected by means of interference filters (20 nm FWHM) and a single channel acquisition was performed. The kinetics at short time delays were fitted by $\int_{-\infty}^{+\infty} g(t-\tau)R(t)\,dt$, i.e. the convolution of the instrumental function $g(t)$ with the response function $R(t)$ having different functional forms according to the processes occurring at specific probe wavelengths (see Section 3). In all the experiments $g(t)$, i.e. the cross-correlation between pump and probe, has a Gaussian shape with time duration of 200 ± 10 fs FWHM for all probe wavelengths.

The sample solutions flew through a 1 mm thick cell equipped with CaF_2 windows and connected to a solution reservoir and a Teflon gear-pump. All the samples were dissolved in acetonitrile and had an optical density of approximately *1* at the excitation wavelength. Steady-state absorption spectra of the solutions were measured before and after the experiments to check for possible sample decomposition. All measurements were carried out at room temperature (∼22°).

Fluorescence lifetimes were measured by directly utilizing the femtosecond pulses extracted from the laser apparatus. The fluorescence was collected by a quartz lens and focussed onto the photocathode of a Hamamatsu R2809U-01 microchannel plate photomultiplier after passing through a proper set of coloured filters (Schott Long Pass WG320 and UG11). The output of the photomultiplier was connected directly to the 50 Ω input of a digital oscilloscope (Tektronix Mod. TDS 7254 2.5 GHz band pass). The overall instrumental function, obtained by measuring the duration of a small leak of the excitation pulse passing through the filters, resulted slightly asymmetric with a time duration (FWHM) of 950 ps (see inset in Fig. 1).

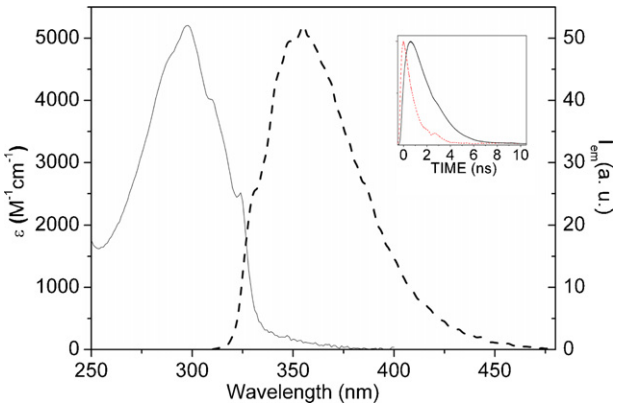

Fig. 1. Steady-state absorption (full line) and emission (dashed line) spectra of the donor (Dn) in acetonitrile. The emission spectrum is obtained by exciting the sample at 305 nm. In the inset: the fluorescence decay (full line) recorded at 360 nm, along with the instrumental function (dotted line).

2.3. Computational methods

To determine the nature of the electronic transitions responsible of the bands appearing in the absorption spectra of Dn and Ac, semiempirical ZINDO [40] calculations were carried out with Gaussian 98 suite of programs [41] on electronic ground state geometries optimized by the RHF method with 6–31 G basis set.

To determine the most stable conformations of the two bichromophores, molecular mechanics simulations (Spartan Software) [42] have been performed with the MMFF94 force field.

3. Results and discussion

3.1. Spectroscopy of the donor (Dn)

The steady-state absorption and emission spectra of molecular Dn in acetonitrile are shown in Fig. 1. The absorption spectrum consists of a broad band centred at 298 nm, whose oscillator strength *f* amounts to 0.060 ± 0.003. The ZINDO calculations indicate that the transitions in this wavelength range have π, π^* character and involve both the naphthalene and the C=O bond of the carboxylic group.

The fluorescence emission of Dn is centered at 355 nm, with a quantum yield $\Phi_F = 0.066 \pm 0.005$ and a lifetime $\tau = 2.05 \pm 0.05$ ns in deoxygenated solutions (see the kinetics in the inset of Fig. 1). The transient spectrum obtained with an excitation at λ = 305 nm shows at 460 nm a weak excited state absorption (ESA) band, distorted by the presence at longer wavelengths of the negative band due to stimulated emission (SE) appearing simultaneously to the excitation process. In the first 2 ps a change of the shape of the ESA band is observed (see Fig. 2); at later delay times its intensity decreases without any appreciable change of its shape. The spectral evolution shown in Fig. 2 and its time scale (∼0.8 ps) are consistent with the occurrence of a vibrational relaxation process in the S_1 level. The relaxed S_1 state converts through internal conversion (IC) and radiative decay to S_0 and through intersystem crossing (ISC) to T_1.

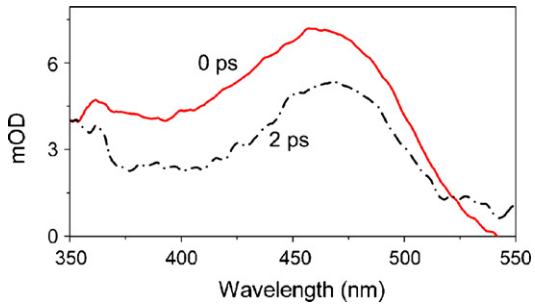

Fig. 2. Transient absorption spectra of the donor in acetonitrile, recorded at pump-probe delays of 0 ps (full line) and 2 ps (dotted–dashed line). The excitation wavelength was 305 nm.

The kinetic constants k_F and $k_{IC} + k_{ISC}$ are calculated from the fluorescence quantum yield and the S_1 lifetime. From $\Phi_F = k_F/(k_F + k_{IC} + k_{ISC})$ and $\tau = 1/(k_F + k_{IC} + k_{ISC})$ we obtain $k_F = (3.3 \pm 0.3) \times 10^7\ s^{-1}$ and $k_{IC} + k_{ISC} = (4.7 \pm 0.4) \times 10^8\ s^{-1}$.

3.2. Spectroscopy of the acceptor (Ac)

Both *f-Ac* and *r-Ac* have been characterized. There are not significant differences between the spectral features of the two chromophores, therefore hereafter their spectral properties are reported referring to a generic Ac compound. Fig. 3 shows the steady-state absorption, emission and fluorescence excitation spectra of Ac measured in acetonitrile.

The absorption spectrum consists of two bands: the first, centered at 482 nm, with an oscillator strength $f = 0.154 \pm 0.008$, and the second, centred at 343 nm, that has an oscillator strength $f = 0.069 \pm 0.003$. Only the emission from the lowest electronic state, centered at 539 nm, is observed, irrespective whether the excitation happens in the first or in the second absorption band. However, the fluorescence quantum yield depends on the excitation wavelength ($\Phi'_F = 0.0076 \pm 0.0005$ at 480 nm, $\Phi''_F = 0.0050 \pm 0.0005$ at 355 nm).

In Fig. 4 transient spectra recorded at different delay times following the excitation at 355 nm are shown. Three main spectral regions can be distinguished: the short wavelength region, where an ESA band is visible; the region between 450 nm and 515 nm, dominated by the bleaching (B) of the ground state and the long wavelength region where a band at 560 nm due to SE is observed. The time evolution of the B band is shown in

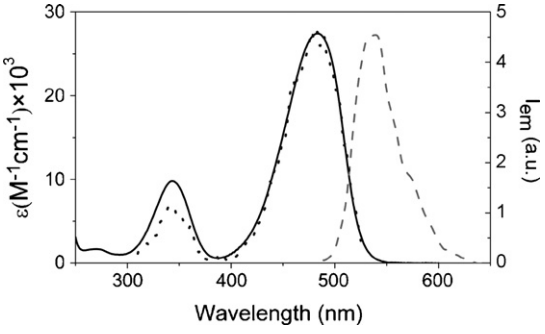

Fig. 3. Steady-state absorption (full line), emission (dashed line) and excitation (dotted line) spectra of Ac in acetonitrile.

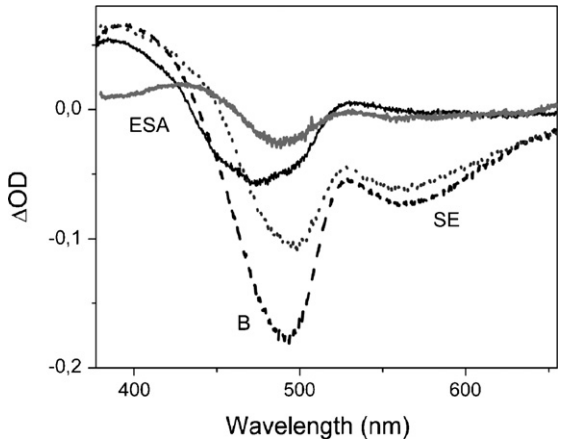

Fig. 4. Transient absorption spectra of the acceptor pumped at 355 nm in acetonitrile, for delay times of 200 fs (solid black line), 1 ps (dashed line), 20 ps (dotted line) and 500 ps (solid gray line). Excited state absorption (ESA) is observed at wavelengths shorter than 450 nm. The strong negative band correspond to the bleaching (B) of the ground state absorption, while the weak negative band is the stimulated emission (SE).

Fig. 5. The ultrafast rise is well-described by the convolution of a step function (instantaneous response) with the instrumental function. A decay follows (shown in the inset of Fig. 5) that can be fitted by a bi-exponential function whose time constants are $\tau_1 = 16 \pm 2$ ps (weight $A_1 = -0.0100 \pm 0.0005$) and $\tau_2 = 218 \pm 19$ ps ($A_2 = -0.0156 \pm 0.0005$).

When exciting at 355 nm, a weak ESA band centered at 530 nm is also observed preceding the appearance of the SE band. The time evolution of the ΔOD signal measured at 570 nm is shown in Fig. 6. The first part consists of an instantaneous absorption contribution whose disappearance entails the growth of the intensity of the emission band. In the first picoseconds the kinetics is well fitted according to the procedure described in Section 2.2 by adopting a response function of the form $R(t) = \theta(t)(A - Be^{-t/\tau_0})$, where $\theta(t)$ is the step function, $A = -0.042 \pm 0.002$, $B = 0.070 \pm 0.003$ and $\tau_0 = 200 \pm 50$ fs. A decay is also observed (see the inset of Fig. 6), fitted by a bi-exponential curve whose parameters are: $A_1 = -0.0009 \pm 0.0002$, $\tau_1 = 25 \pm 8$ ps and $A_2 = 0.0040 \pm 0.0001$, $\tau_2 = 214 \pm 22$ ps.

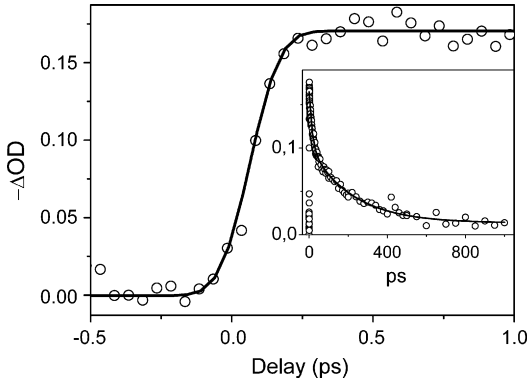

Fig. 5. Time dependence of the bleaching (B) recorded at 490 nm for Ac in acetonitrile over short delay times. The long delay time behavior is shown in the inset.

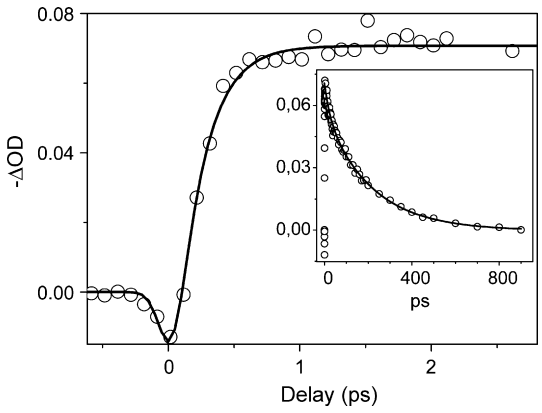

Fig. 6. Time dependence of the stimulated emission (SE) recorded at 570 nm for the acceptor in acetonitrile over short delay times. The long delay time behavior is shown in the inset.

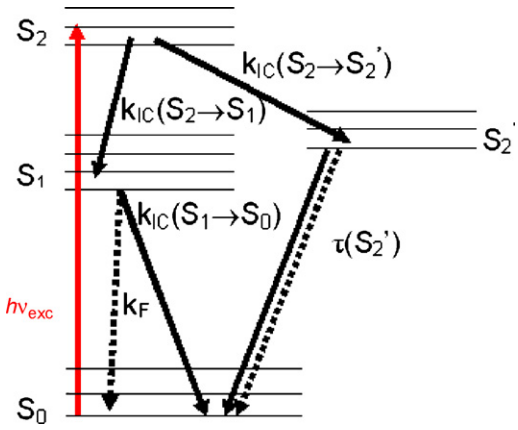

Scheme 1. Jablonski diagram showing the electronic states relevant to the experiment and the relaxation paths of Ac molecule.

The unambiguous interpretation of the time evolution of the red portion of the transient spectra is achieved by exciting Ac S_1 state at 480 nm: the instantaneous transient absorption component, centered at 530 nm, disappears. Between 530 and 650 nm, only the SE band is observed, and its decay is well fitted by a single exponential with $\tau_2 = 194 \pm 14$ ps. From the latter observation one can conclude that the weak absorption band, centered at 530 nm, is due to ESA from the S_2 state, that has a lifetime of about 200 fs and decays into two states: the S_1 state, with a lifetime of ~200 ps and a "dark" state (hereinafter labelled as S_2'), not appearing in the steady-state absorption spectrum, with a lifetime of ~20 ps.

The presence of an electronic state, optically not active but involved in the electronic relaxation dynamics, such as S_2' in Ac, was already reported in other 4-amino-7-nitrobenz-2-oxa-1,3-diazole derivatives [43].

The absorption band appearing in the blue portion of the transient spectra exhibits a time evolution consisting of an initial fast growth, followed by a much slower decay. The decay has mono-exponential character, with a lifetime $\tau = 191 \pm 11$ ps. The overall time evolution of the absorption band centered at 390 nm makes straightforward its assignment to the S_1 state, that is populated in ~200 fs when Ac S_2 is excited, and that has a lifetime $\tau(S_1)$ ~200 ps.

The results concerning Ac photophysics can be summarized according to the Jablonski diagram depicted in Scheme 1.

From $\Phi_F' = k_F/(k_F + k_{IC}(S_1 \rightarrow S_0))$, and from the S_1 state lifetime, the fluorescence kinetic constant k_F is evaluated:

$$k_F = \Phi_F'[k_F + k_{IC}(S_1 \rightarrow S_0)] = \frac{\Phi_F'}{\tau(S_1)} = (3.8 \pm 0.4) \times 10^7\ s^{-1} \quad (3)$$

The value of $k_{IC}(S_1 \rightarrow S_0)$ for the internal conversion process can be determined:

$$k_{IC}(S_1 \rightarrow S_0) = \frac{1}{\tau(S_1)} - k_F = (5.0 \pm 0.2) \times 10^9\ s^{-1} \quad (4)$$

The fluorescence quantum yield, upon S_2 state excitation, is given by:

$$\Phi_F'' = \frac{k_F k_{IC}(S_2 \rightarrow S_1)}{[k_{IC}(S_2 \rightarrow S_1) + k_{IC}(S_2 \rightarrow S_2')][k_{IC}(S_1 \rightarrow S_0) + k_F]} = \Phi_F' \Phi_{IC}(S_2 \rightarrow S_1); \quad (5)$$

by knowing the values of Φ_F' and Φ_F'', Φ_{IC} $(S_2 \rightarrow S_1)$ can be determined:

$$\Phi_{IC}(S_2 \rightarrow S_1) = \frac{\Phi_F''}{\Phi_F'} = 0.7 \pm 0.1 \quad (6)$$

Therefore, the kinetic constant for the internal conversion process from S_2 to S_1 can be evaluated:

$$k_{IC}(S_2 \rightarrow S_1) = \frac{\Phi_{IC}(S_2 \rightarrow S_1)}{\tau(S_2)} = (3 \pm 1) \times 10^{12}\ s^{-1} \quad (7)$$

The ZINDO calculations predict the contribution of three main electronic transitions to Ac ground-state absorption spectrum. The first transition, having the largest oscillator strength value, gives rise to a band centered at 424 nm ($f = 0.51$): it has charge transfer character, in which the amino group acts as a donor and the remaining conjugated system containing the electron-drawing nitro group acts as an acceptor. This calculated transition can be interpreted as responsible for the most intense band observed in the spectrum at 482 nm. A second weaker band should appear at 339 nm ($f = 0.089$): it is due to an electronic transition having charge transfer character, where the amino group acts as a donor and a conjugated system limited to the heterocyclic oxadiazol ring, along with the nitro group, acts as an acceptor. This transition can be associated with the band experimentally observed at 343 nm. Finally, the calculations predict a third transition, of much weaker intensity, having $n \rightarrow \pi^*$ character: it involves an n-orbital of the nitro group, lying on the molecular plane defined by the two condensated rings, and a π^* orbital extended over the entire conjugated system. Its energy is higher than that of the S_1 state, with a transition wavelength of 340 nm and an oscillator strength $f = 0.0238$. This transition can be identified as due to the 'dark' state S_2', a state that cannot be perceived directly from the steady-state absorption spectrum, but whose existence is proved by the wavelength-dependent fluorescence quantum yield and by the relaxation dynamics of Ac investigated through TAS.

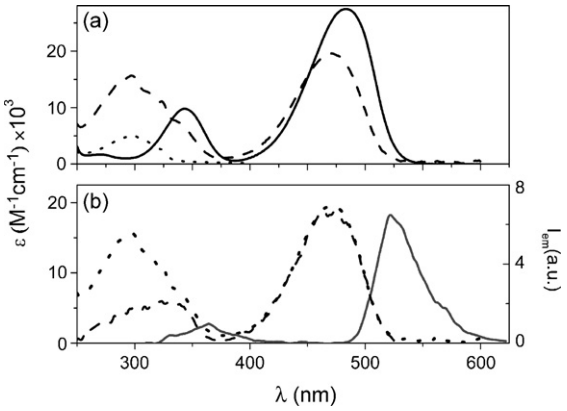

Fig. 7. (a) The absorption spectra of Ac (full line), of Dn (dotted line) and of the ***f-Bi*** (dashed line); (b) The absorption (dotted line), the emission with $\lambda_{exc} = 300$ nm (full line) and the excitation with $\lambda_{em} = 535$ nm (dashed line) spectra of ***f-Bi***.

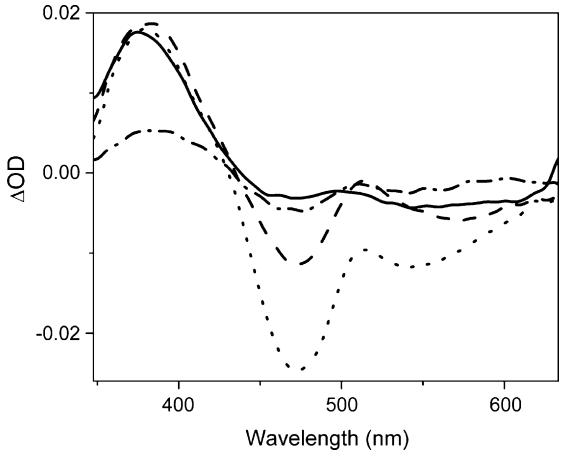

Fig. 8. Transient absorption spectra of ***f-Bi*** excited at $\lambda = 305$ nm in acetonitrile, for delay times of 300 fs (full line), 1 ps (dashed line), 50 ps (dotted line) and 1 ns (dashed–dotted line).

3.3. The flexible bichromophore (*f-Bi*)

3.3.1. Absorption and emission properties

In Fig. 7a, the steady-state absorption spectra of ***f-Bi***, Ac and Dn, recorded in acetonitrile, are compared. When the donor and acceptor chromophores are covalently linked in ***f-Bi***, they interact appreciably. The bands associated to Ac undergo an ipochromism (i.e. ε, the molar extinction coefficient decreases of ∼30%) and an ipsochromism (i.e. the bands shift to the blue of ∼14 nm), whereas the characteristic band of Dn, in the UV region, exhibits an iperchromism effect (i.e. ε of ***f-Bi*** at 298 nm is larger than $2\varepsilon_D + \varepsilon_A$ estimated from the absorption spectra of the molecular chromophores).

The emission properties of ***f-Bi*** are shown in Fig. 7b. Independently on the excitation wavelength, ***f-Bi*** exhibits the emission from the lowest excited state of the acceptor chromophore, giving rise to the band centered at 523 nm. This means that, whether Ac is directly excited or not, its emission is always detectable. It can be inferred that in ***f-Bi*** energy transfer from Dn to Ac surely occurs. Moreover ***f-Bi*** exhibits dual fluorescence, similarly to other bichromophoric compounds [44,45]. In fact, when ***f-Bi*** is excited upon UV irradiation, a very weak additional emission band is observed at 363 nm. On the basis of its position it can be attributed to a residual fluorescence of Dn, not quenched by the EET process. In Table 1 the fluorescence quantum yields of ***f-Bi*** along with those of ***r-Bi*** are reported for different excitation wavelengths.

Table 1
Fluorescence quantum yield of ***f-Bi*** and ***r-Bi*** at various excitation wavelengths

λ_{exc} (nm)	Residual Φ_F of Dn in ***f-Bi***	Φ_F of Ac in ***f-Bi***	Φ_F of Ac in ***r-Bi***
300	0.00067 ± 0.00007	0.0088 ± 0.0005	0.034 ± 0.002
313	0.00065 ± 0.0001	0.0110 ± 0.0006	0.038 ± 0.002
325		0.0140 ± 0.0006	0.043 ± 0.002
339		0.0180 ± 0.0006	0.050 ± 0.002
350		0.0180 ± 0.0006	0.070 ± 0.002
470		0.0240 ± 0.0006	

3.3.2. Ultrafast experiments

At 305 nm, the main contribution to the molar extinction coefficient of ***f-Bi*** arises from the two donor chromophores. Transient spectra, collected at different delay times, are shown in Fig. 8. They look similar to those measured in molecular Ac.

In order to interpret the complex features of the transient spectra of ***f-Bi***, both the acceptor and donor contributions must be taken into account. Dn gives rise to a weak transient absorption band, extended between 350 and 540 nm, with a maximum at 470 nm. On the other hand, Ac is expected to originate (1) an ESA band in the blue region of the transient spectra, due to the S_1 state; (2) a B band with negative values of ΔOD in correspondence of the $S_0 \rightarrow S_1$ transition and finally, (3) two bands, with opposite sign, in the red portion of the spectra: a weak absorption, due to the ESA from S_2 state, and a SE band.

These spectral features are responsible for different dynamics measured in the three spectral regions. In Fig. 9a, the kinetics recorded at 480 nm is reported. The time evolution of ΔOD at this wavelength consists of two parts: the rising signal occurring within the first 20 ps, followed by a decay on ns time scale. The first part of the kinetics is fitted by the convolution of the instrumental function with

$$R(t) = \theta(t)[A + B(1 - e^{-t/\tau_{ET}}) + C(e^{-t/\tau_{Dn}})] \quad (8)$$

From the fitting procedure $A = -0.013 \pm 0.001$, $B = -0.016 \pm 0.001$, $\tau_{ET} = 3.5 \pm 0.2$ ps, $C = +0.013 \pm 0.001$ and $\tau_{Dn} = 0.65 \pm 0.05$ ps. The decay part is reproduced by a bi-exponential function having $\tau_1 = 25 \pm 7$ ps, $\tau_2 = 404 \pm 40$ ps and $A_1 = -0.014 \pm 0.003$, $A_2 = -0.0212 \pm 0.0006$. At 480 nm, Ac gives rise to a B band; on the contrary Dn contributes with an ESA band. The first two terms in Eq. (8) account for the fact that Ac is excited through two different mechanisms. The term A derives from the fraction of Ac molecules excited "instantaneously". This can be due to either a direct excitation of Ac, partially absorbing at $\lambda = 305$ nm or to a coherent excitonic mechanism of energy transfer, detected, so far, in some other bichromophoric and dendrimeric species [46–48]. The second term of Eq. (8) indicates that the most relevant part of Ac

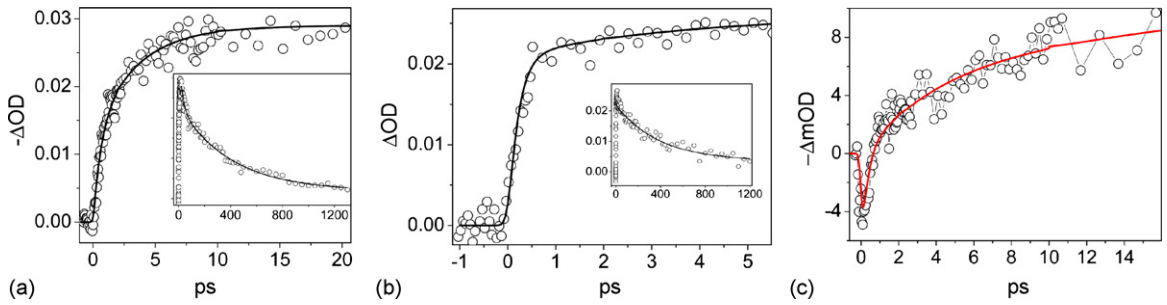

Fig. 9. Time dependence of (a) the bleaching B recorded at λ = 480 nm, (b) the ESA at λ = 380 nm and (c) the SE at λ = 550 nm, for ***f-Bi*** in acetonitrile at short delay times. The decay time in the nanosecond regime is shown in the insets.

molecules, are excited through a slower mechanism, i.e. the energy transfer. The third term of Eq. (8) highlights that Dn has a lifetime of $\tau_{Dn} = 0.6 \pm 0.2$ ps. This fairly short lifetime of Dn derives from two contributions: (1) the intrachromophore vibrational relaxation process occurring on the sub-picosecond time regime (see Section 3.1), and (2) the Dn → Ac energy transfer, having $\tau_{ET} = 3.5 \pm 0.2$ ps.

The bi-exponential nature of the decay points out that the Ac S_0 recovery occurs through two different intermediate states: one with a lifetime $\tau_1 \sim 25$ ps, and the other with $\tau_2 \sim 400$ ps. By analogy with the relaxation dynamics of molecular Ac, the first term can be attributed to a relaxation process due to the optically inactive S_2'. The second term can be identified with the decay of the fluorescent S_1 state, showing a longer lifetime in ***f-Bi*** than in molecular Ac. This result is also confirmed by the larger emission quantum yield of ***f-Bi***.

The absorption band centered at λ = 379 nm, extending over the blue and near-UV regions of the transient spectra, evolves similarly (see Fig. 9b). Its rise is well-described by the convolution of the instrumental function with:

$$R(t) = \theta(t)[A(1 - e^{-(t/\tau_0)}) + B(1 - e^{-(t/\tau_{ET})})] \quad (9)$$

The fitting provides the following values: $\tau_0 = 200 \pm 50$ fs, $A = 0.0200 \pm 0.001$, $\tau_{ET} = 3.5 \pm 0.2$ ps and $B = 0.0050 \pm 0.0005$. Since the band at λ = 379 nm is due to an absorption of the Ac S_1 state, Eq. (9) reveals that this state is produced through two different paths. The first faster route is characterized by the lifetime $\tau_0 \sim 200$ fs, and the second route has a longer lifetime of ∼3.5 ps. In agreement with the relaxation dynamics of the molecular Ac, the first path can be attributed to the internal conversion from S_2 to S_1 of Ac. As in the transient measured at λ = 480 nm it is observed that a fraction of Ac S_2 states is generated within an interval as short as the instrumental time resolution, the rest is excited through a slower energy transfer mechanism, requiring roughly 10 ps (long enough to mask the faster Ac $S_2 \rightarrow S_1$ internal conversion).

The decay of the signal at λ = 379 nm (see inset of Fig. 9b) is mono-exponential with a time constant $\tau_2 = 395 \pm 50$ ps, in agreement with the lifetime obtained from the kinetics at 480 nm.

The picture emerging from the kinetics analyzed so far is confirmed by the interpretation of the kinetics recorded at λ = 550 nm (see Fig. 9c). At this wavelength, three main electronic transitions contribute to the time evolution of the ΔOD: the absorption of the S_2 state and the emission from the S_2' and S_1 states. Therefore,

$$R(t) = \theta(t)[A(B - e^{-(t/\tau_0)}) + C(D - e^{-(t/\tau_0)})(1 - e^{-(t/\tau_{ET})}) + E(e^{-(t/\tau_1)})] \quad (10)$$

The fitting process of the experimental data with Eq. (10) provides the following results: $A = -0.004 \pm 0.001$, $B = 1.5$, $\tau_0 = 200 \pm 50$ fs, $C = -0.092 \pm 0.005$, $D = 0.06 \pm 0.003$, $\tau_{ET} = 3.5 \pm 0.2$ ps, $E = 0.007 \pm 0.001$ and $\tau_1 = 20 \pm 4$ ps.

In order to clarify which process is responsible of the ultrafast S_2 formation, ***f-Bi*** has been excited also at λ = 290 nm. At this wavelength Ac has a smaller molar extinction coefficient than at λ = 305 nm ($\varepsilon(Ac)_{290} = 870\ cm^{-1}\ M^{-1}$ compared to $\varepsilon(Ac)_{305} = 2376\ cm^{-1}\ M^{-1}$) [49], whereas the molar extinction coefficient of the two Dn chromophores is larger than that at λ = 305 nm ($2\varepsilon(Dn)_{290} = 13562\ cm^{-1}\ M^{-1}$ and $2\varepsilon(Dn)_{305} = 10938\ cm^{-1}\ M^{-1}$). Therefore, if the Ac S_2 state is produced by direct absorption of radiation, its contribution to the rise of the signal is expected to decrease when the sample is irradiated at λ = 290 nm. In Fig. 10 the kinetics recorded at λ = 480 nm, for excitation at λ = 305 and λ = 290 nm, are compared.

By excitation at λ = 305 nm, the negative contribution to ΔOD of the bleaching of the $S_1 \rightarrow S_0$ transition of Ac is large

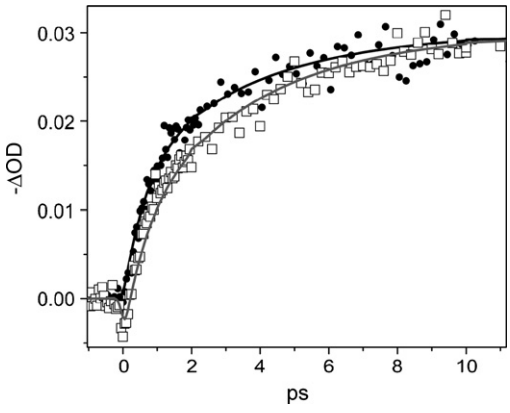

Fig. 10. Time dependence of the bleaching B recorded at λ = 480 nm for ***f-Bi*** excited at two different excitation wavelengths in acetonitrile: at $\lambda_{exc} = 305$ nm (full circles fitted by the full black line) and at $\lambda_{exc} = 290$ nm (empty squares fitted by the full gray line).

enough to mask the absorption contribution by the Dn chromophores. On the other hand, when ***f-Bi*** is excited at $\lambda = 290$ nm, the situation is opposite and the absorption contribution due to Dn dominates. By fitting the two kinetics with the response function of Eq. (8), it is possible to quantitatively determine the weight of the different contributions and to compare them. Since the coefficient C of Eq. (8) depends on the molar extinction coefficient of the Dn excited state (which is unknown), it is necessary to compare the $|A|$ and $|B|$ terms, which are proportional to ε_{Ac} and $2\varepsilon_{Dn}\Phi_{Dn}$, respectively, in the hypothesis that the instantaneous population of Ac is due to its direct excitation, whereas the slower route of Ac production is due to intra-EET, with a lifetime of ~3.5 ps. Going from $\lambda = 305$–290 nm the contribution represented by |A| decreases of a factor ~2 with respect to |B|. This decrease is quantitatively consistent with a reduction of 1.6 ± 0.1 of ε_{Ac} compared to the term $2\varepsilon_{Dn}\Phi_{Dn}$. Therefore, it seems reasonable to conclude that the instantaneous population of a fraction of Ac in ***f-Bi*** is due to its direct excitation.

3.3.3. Determination of the kinetic constants

The data collected for ***f-Bi*** allow us to propose the complete picture of the relaxation dynamics graphically portrayed in Scheme 2.

The kinetic constant for the EET in ***f-Bi*** is given by:

$$k_{ET} = \frac{1}{\tau_{ET}} = (2.8 \pm 0.2) \times 10^{11}\ s^{-1} \quad (11)$$

Since k_{ET} is fairly larger than the sum of the kinetic constants describing the competitive decay paths in Dn, it is a clear-cut that the quantum efficiency for the energy transfer (Q) is almost equal to 1:

$$Q = \frac{k_{ET}}{k_{ET} + (k_F + k_{IC} + k_{ISC})_{Dn}} = 0.998 \quad (12)$$

There is a last point to be outlined. ***f-Bi*** emission spectra show a weak but measurable emission from Dn (see Fig. 7b). In Table 1 it is reported $\Phi_F(Dn) = 0.00067$, value which is consistent, within the error, with the EET quantum efficiency. However, it must be observed that the numerical evaluation of Q is made by utilizing the molecular Ac and Dn spectroscopic data and therefore the outcome of the iperchromic effect in ***f-Bi*** is not taken into account. This latter cannot be quantitatively included in the calculations but its effect must be that of slightly reducing the Q-value. This observation further justifies the presence of a residual Dn emission in ***f-Bi***.

From the fluorescence quantum yield of ***f-Bi***, and from the value of the S_1^{Ac} lifetime, it is possible to determine the fluorescence kinetic constant according to Eq. (3): $k_F^{Ac} = (6.0 \pm 0.6) \times 10^7\ s^{-1}$. Subsequently $k_{IC}^{Ac}(S_1 \rightarrow S_0) = (2.4 \pm 0.2) \times 10^9\ s^{-1}$.

Furthermore, when ***f-Bi*** is excited at $\lambda = 339$ nm or $\lambda = 350$ nm, only S_2^{Ac} is populated, since Dn does not absorb at these wavelengths. Therefore, the resulting fluorescence quantum yield is related exclusively to the relaxation dynamics of Ac in ***f-Bi***. According to Eq. (5) $\Phi_{IC}(S_2 \rightarrow S_1) = 0.75 \pm 0.04$. By knowing the S_2^{Ac} lifetime, according to Eq. (7) it is possible to evaluate the kinetic constant of the internal conversion from S_2 to S_1: $k_{IC}^{Ac}(S_2 \rightarrow S_1) = (3.8 \pm 0.8) \times 10^{12}\ s^{-1}$.

The kinetic constants for the decay of Ac in ***f-Bi*** and in the molecular Ac solution are in general quite similar, the only appreciable difference involving the S_1 state, whose lifetime in ***f-Bi*** is about twice longer then in isolated Ac.

3.4. The rigid bichromophore (*r-Bi*)

3.4.1. Absorption and emission properties

In Fig. 11a the steady-state absorption spectrum of ***r-Bi*** along with that of ***f-Bi*** are shown. The only differences between ***f-Bi*** and ***r-Bi*** absorption spectra regard the reduced values of Dn molar extinction coefficients in ***r-Bi*** and a slightly reduced blue-shift for the Ac band associated to the $S_0 \rightarrow S_2$ transition. This latter feature should result advantageous for the efficiency of intra-EET processes.

In Fig. 11b, the emission properties of ***r-Bi*** are also shown. As in the case of ***f-Bi*** the emission derives from the lowest excited state of Ac thus suggesting that also in this case the energy transferred is the most efficient process.

A comparison between the fluorescence quantum yields of ***r-Bi*** and ***f-Bi*** as a function of excitation wavelengths is reported in Table 1 (see Section 3.3.1). The first observation is that the Φ_F

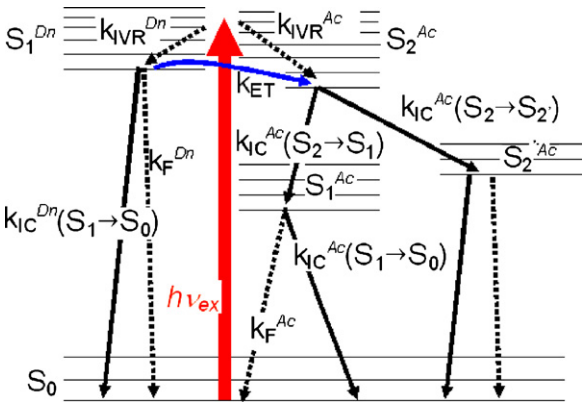

Scheme 2. Jablonski diagram showing the electronic states and the relaxation paths for both ***f-Bi*** and ***r-Bi*** molecules.

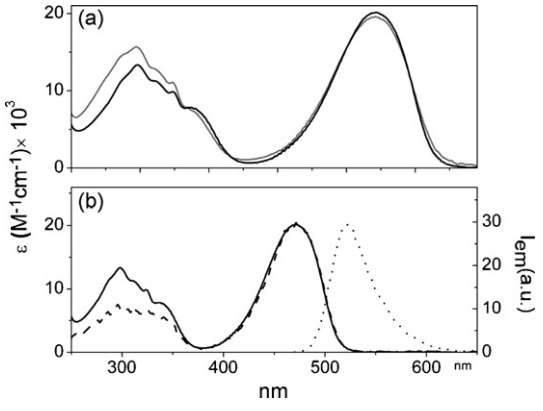

Fig. 11. In (a), the absorption spectra of ***r-Bi*** (black line) and of ***f-Bi*** (gray line) are shown; in (b), the absorption (full line), the emission with $\lambda_{exc} = 460$ nm (dotted line) and the excitation with $\lambda_{em} = 540$ nm (dashed line) spectra of ***r-Bi***, are depicted. All the spectra are recorded in acetonitrile.

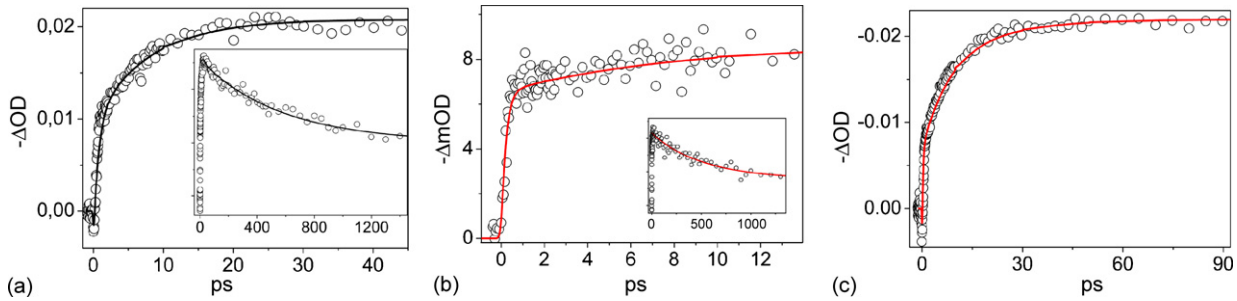

Fig. 12. Time dependence of (a) the bleaching B recorded at λ = 480 nm, (b) the ESA at λ = 380 nm and (c) the SE at λ = 550 nm, for ***r-Bi*** in acetonitrile at short delay times. The decay time in the nanosecond regime is shown in the insets.

values for ***r-Bi*** are three times larger than those for ***f-Bi*** and this should be due to the skeletal rigidity in ***r-Bi*** which reduces the loss of excitation energy through non-radiative pathways. Moreover, the residual fluorescence of Dn is absent in ***r-Bi***, whereas it is detectable in ***f-Bi*** (see Fig. 7b).

3.4.2. Time resolved experiments

The number and the kind of bands appearing in the transient spectra of ***r-Bi*** are equivalent to those recorded for ***f-Bi***.

In Fig. 12a the kinetics at λ = 480 nm is reported. Similarly to the case of ***f-Bi***, the kinetics can be divided in two parts: the first part (within the first 40 ps) where the absolute value of ΔOD rises until it reaches a plateau and a second part characterized by a slower decay. The growth is well-described by the convolution of the instrumental function with a response function of the same form of Eq. (9); the fitting gives the following parameters: $A = -0.016 \pm 0.001$, $B = -0.018 \pm 0.001$, $\tau_{ET} = 8.0 \pm 0.5$ ps, $C = +0.020 \pm 0.001$, $\tau_{Dn} = 0.73 \pm 0.05$ ps. The decay part is fitted by a bi-exponential function having $A_1 = -0.002 \pm 0.001$, $A_2 = -0.012 \pm 0.001$, $\tau_1 = 20 \pm 7$ ps, and $\tau_2 = 570 \pm 60$ ps. As in the case of ***f-Bi*** also in ***r-Bi*** direct excitation of Ac occurs upon excitation at λ = 305 nm.

In ***r-Bi*** the energy transfer from Dn to Ac occurs with a time constant of ∼8.0 ps. Due to the fairly short lifetime of Dn, only Ac contributes to the decay portion of the kinetics. Ac relaxes to the electronic ground state through two parallel pathways with time constants of ∼20 ps and ∼570 ps, respectively. By analogy with the relaxation dynamics of pure Ac and of ***f-Bi***, the first path can be identified with the $S'_2 \rightarrow S_0$ internal conversion, whereas the second path can be attributed to the $S_1 \rightarrow S_0$ internal conversion. The S_1 state shows an increase of its lifetime passing from pure Ac to ***f-Bi*** and to ***r-Bi***, in perfect agreement with the trend of the fluorescence quantum yields.

For the band centered at 380 nm, the temporal evolution of the ΔOD signal also consists of two different parts (see Fig. 12b). The growth is reproduced by the convolution of the instrumental function with a response given by Eq. (10) with $\tau_0 = 200 \pm 20$ fs, $A = 0.006 \pm 0.001$, $\tau_{ET} = 8.0 \pm 0.5$ ps and $B = 0.002 \pm 0.0005$. On the other hand, the decay is well-fitted by a mono-exponential function having $\tau_2 = 510 \pm 80$ ps. Since the band at λ = 380 nm is due to the S_1 state of Ac, the two terms (*A* and *B*) represent two different routes of S_1 production: the fastest rate is associated to internal conversion $S_2 \rightarrow S_1$, the slower is due to the energy transfer from Dn (S_1) to Ac (S_2).

The response function in the red part of the spectrum (550 nm) is given by Eq. (10), with $A = -0.019 \pm 0.001$, $B = 1.0 \pm 0.1$, $\tau_0 = 200 \pm 20$ fs, $C = -0.17 \pm 0.01$, $D = 0.1 \pm 0.01$, $\tau_{ET} = 8.0 \pm 0.5$ ps, $E = 0.008 \pm 0.001$ and $\tau_1 = 20 \pm 5$ ps (see Fig. 12c). As in the case of ***f-Bi***, two paths for the population decay of S_2 state of Ac can be identified: the first one is instantaneous and is due to the direct excitation of Ac chromophore; the second, occurring on a slower time scale, is due to the energy transfer from Dn to Ac. The S_2 state has a lifetime $\tau_0 = 200 \pm 50$ fs and it gives rise to S'_2 state whose lifetime is ∼20 ps, to S_1 state, whose lifetime is $\tau_2 \sim 540$ ps.

3.4.3. Determination of the kinetic constants

The Jablonski diagram representing the relaxation dynamics after photo-excitation of ***r-Bi*** is qualitatively equivalent to that proposed for ***f-Bi*** and depicted in Scheme 2 (see Section 3.3.3). The relaxation mechanisms of ***f-Bi*** and ***r-Bi*** are the same, with some differences in the rates of the relaxation pathways. An overall comparison of the relaxation dynamics and energy transfer rates between the two bichromophore species can be made on the basis of the data collected in Table 2, where the averaged values of the lifetimes of the excited states of the acceptor chromophore in ***r-Bi***, ***f-Bi*** and molecular Ac, along with the energy transfer time constants are reported.

It is evident that the main differences concern the S_1^{Ac} lifetime in the three species and the energy transfer time constant in the two bichromophoric compounds.

The difference in $\tau(S_1^{Ac})$ is obviously reflected in distinct values for the kinetic constants of the processes involved in the decay of the S_1 state. By applying Eqs. (3) and (4), the k_F^{Ac} and k_{IC}^{Ac} (S_1) values for ***r-Bi*** can be determined. They are reported in Table 3, along with the other kinetic constants, associated with the relaxation routes of the S_2 state evaluated through the use of Eqs. (5)–(7). For comparison, the values of the same

Table 2
Averaged lifetimes (in ps) of the electronic excited states of acceptor chromophore in Ac, ***f-Bi***, ***r-Bi*** and averaged energy transfer lifetime in ***f-Bi*** and ***r-Bi***

	$\tau(S_2^{Ac})$	$\tau(S'^{Ac}_2)$	$\tau(S_1^{Ac})$	τ_{ET}
Ac	0.20 ± 30	20 ± 6	200 ± 20	
f-Bi	0.20 ± 30	22 ± 5	400 ± 555	3.5 ± 0.2
r-Bi	0.20 ± 30	20 ± 5	540 ± 70	8.0 ± 0.5

Table 3
Kinetic constants associated with the different decay paths of acceptor chromophore in pure Ac, ***f-Bi*** and ***r-Bi*** along with the energy transfer kinetic constant

	$k_{IC}^{Ac}(S_2 \rightarrow S_1)$ (s^{-1})	$k_{IC}^{Ac}(S_1 \rightarrow S_0)$ (s^{-1})	k_F^{Ac} (s^{-1})	k_{ET} (s^{-1})
Ac	$(3.3 \pm 1) \times 10^{12}$	$(4.6 \pm 0.3) \times 10^{9}$	$(3.8 \pm 0.4) \times 10^{7}$	
f-Bi	$(3.8 \pm 0.8) \times 10^{12}$	$(2.4 \pm 0.3) \times 10^{9}$	$(6.0 \pm 0.6) \times 10^{7}$	$(2.86 \pm 0.16) \times 10^{11}$
r-Bi	$(3.55 \pm 0.78) \times 10^{12}$	$(1.7 \pm 0.18) \times 10^{9}$	$(1.3 \pm 0.2) \times 10^{8}$	$(1.25 \pm 0.08) \times 10^{11}$

kinetic constants for Ac and ***f-Bi*** are also reported. As expected, the $k_{IC}^{Ac}(S_2 \rightarrow S_1)$, $k_{IC}^{Ac}(S_2 \rightarrow S_2')$ kinetic constants of the three species do not differ appreciably. On the other hand, isolated Ac exhibits the largest $k_{IC}^{Ac}(S_1 \rightarrow S_0)$, and the lowest k_F^{Ac} values, entailing the least Φ_F'. ***r-Bi*** shows the slowest $S_1 \rightarrow S_0$ internal conversion process and the largest k_F value, implying the highest Φ_F'.

As far as the energy transfer process is concerned, ***f-Bi*** has a k_{ET} about two times larger than ***r-Bi***. The quantum efficiency Q of intra-EET in ***r-Bi*** is 0.996.

3.5. The mechanism of the electronic energy transfer

The data discussed above highlight a very fast and efficient intramolecular EET process occurring in both ***f-Bi*** and ***r-Bi***. It is important to model the mechanism(s) responsible of the intra-EET, in other words the way Dn and Ac moieties interact in the two bichromophoric compounds and the way structural differences can affect the interaction.

Since in ***f-Bi*** and ***r-Bi*** the aromatic rings of Dn and Ac are linked to each other by saturated σ bonds, the contribution to the energy transfer process of the through-bond exchange interaction mechanism is negligible. Hence it is reasonable to apply the Förster theory [50,51] to describe the very fast intra-EET. The Förster theory entails a dipole–dipole induced coulombic resonant interaction between Dn and Ac. According to this theory, the rate of energy transfer (k_{ET}) is given by

$$k_{ET} = \frac{9000 \ln(10) \kappa^2 \Phi_{Dn} J_{res}}{128 \pi^5 n^4 N_A \tau_{Dn} R_{Ac-Dn}^6} \quad (13)$$

where κ^2 is the orientation factor, Φ_{Dn} and τ_{Dn} are the fluorescence quantum yield and lifetime of Dn, respectively, n the refractive index of the solvent, N_A the Avogadro's number, R_{Ac-Dn} the interchromophoric distance and J_{res} is the spectral overlap integral for the resonance interaction, whose definition is given by:

$$J_{res}(dm^3\ mol^{-1}\ cm^3) = \int_0^\infty \frac{\bar{F}_{Dn}(\bar{\nu}) \varepsilon_{Ac}(\bar{\nu})\, d\bar{\nu}}{\bar{\nu}^4} \quad (14)$$

In Eq. (14), $\bar{F}_{Dn}(\bar{\nu})$ is the normalized emission spectrum of Dn and $\varepsilon_{Ac}(\bar{\nu})$ is the molar extinction coefficient of Ac in the two species, [49] expressed in $dm^3\ mol^{-1}\ cm^{-1}$. In the present case, $J_{res} = 3.11 \times 10^{-16}\ mol^{-1}\ cm^6$ for ***f-Bi*** and $3.5 \times 10^{-16}\ mol^{-1}\ cm^6$ for ***r-Bi***. All the terms appearing in Eq. (13) are known, except for κ^2 and $R_{Ac\text{-}Dn}$. To assign a value to κ^2 factor, it is necessary to figure out how Dn and Ac moieties are mutually oriented. The orientational factor is given by:

$$\kappa = \sin\theta_{Dn} \sin\theta_{Ac} \cos\varphi - 2\cos\theta_{Dn} \cos\theta_{Ac} \quad (15)$$

where θ_{Dn} and θ_{Ac} are the angles that transition dipole moments of Dn and Ac, respectively, make with the interchromophore separation vector R_{Dn-Ac}, and φ is the dihedral angle defined by the corresponding three vectors. The value of κ^2 can vary between 0 and 4. Since in the two bichromophoric species the link between Dn and Ac is flexible, it is reasonable to assume that they are randomly oriented therefore providing $\kappa^2 = 2/3$. Under this assumption and by inserting the experimentally determined value of k_{ET} in Eq. (13), the interchromophoric distance R_{Dn-Ac}, at which the energy transfer occurs, can be determined. It follows that R_{Dn-Ac} is 4.3 Å in ***f-Bi*** and 5.0 Å in ***r-Bi***: only at these short distances the energy transfer can occur as fast as observed. In the Förster approach, the upper limit of the interchromophoric distance R_{Ac-Dn}^0 for an observable energy transfer can be obtained from the relation $k_{ET} \times \tau_{Dn} = 1$, i.e. the intra-EET rate constant is equal to the reciprocal of the molecular donor lifetime. In this case the interchromophoric distance would be equal to 12.4 Å.

In order to confirm that the interchromophoric distance R_{Ac-Dn} calculated by applying the Föster theory is physically consistent, molecular mechanics calculations were carried out on both ***f-Bi*** and ***r-Bi***. Two possible conformations are predicted as the most stable, corresponding to different orientations of the two donor chromophores respect to the acceptor chromophore. In one of these conformations, the transition dipole moments of donor and acceptor are parallel to each other and to the Dn–Ac interchromophoric axis, and their distance is maximum (we will refer to this as the "collinear conformation"). In the other conformation the dipoles are orthogonal to the donor–acceptor interchromophoric axis and their distance is minimum ("cofacial conformation"). These two conformations are portrayed in Fig. 13.

In the collinear conformation, the average interchromophoric distance is $R_{Dn-Ac} \approx 12$ Å (estimated from the position of the center of mass of the free chromophores in both the bichromophores) and, since $\theta_{Dn} = \theta_{Ac} = 0$ and $\varphi = 0$, $\kappa^2 = 4$. In the cofacial conformation, $R_{Dn-Ac} \approx 5$ Å and, since $\theta_{Dn} = 90°$, $\theta_{Ac} = 90°$ and $\varphi = 0$, $\kappa^2 = 1$. We can then estimate the intra-EET kinetic constant for the two conformations in both ***f-Bi*** and ***r-Bi***. For the collinear conformation, $k_{ET} \approx 3.7 \times 10^9\ s^{-1}$ is about two orders of magnitude less than the experimental values. For the cofacial conformation in ***f-Bi*** the calculated k_{ET} is $1.76 \times 10^{11}\ s^{-1}$ and in ***r-Bi*** is $3.7 \times 10^{11}\ s^{-1}$. The order of magnitude is in agreement with that experimentally derived values for both the compounds. However, we observe that the distances obtained by the molecular mechanics calculations are not significantly different in the two bichromophores. The difference between the rates of the EET process derives essentially from the overlap between the Dn emission and the Ac absorption which

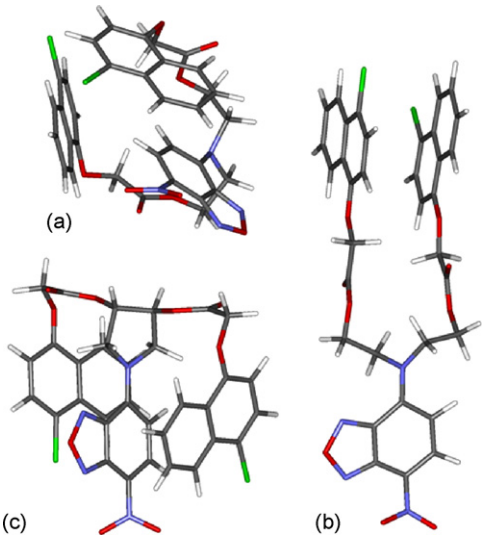

Fig. 13. The most stable conformations of ***f-Bi*** and ***r-Bi***: (a) cofacial and (b) collinear conformations of ***f-Bi*** and (c) the cofacial conformation of ***r-Bi***.

is better in the case of ***r-Bi***, thus leading to a higher rate in the latter.

It is evident that, although the bichromophores exist in solution at room temperature as a distribution of several conformations, the fast intramolecular energy transfer measured in our experiments is due only to the cofacial conformation (see Fig. 13a and c).

4. Conclusions

Steady-state and time-resolved absorption and fluorescence spectroscopic properties of Dn, Ac, ***f-Bi*** and ***r-Bi*** molecules, show that rapid and efficient intra-EET processes occur in the two bichromophoric species. The ensemble of spectroscopic data collected gives a complete picture of the relaxation and energy transfer processes and provides a quantitative estimate of the corresponding kinetic constants. Being Dn and Ac linked through saturated C–C σ bonds in both ***f-Bi*** and ***r-Bi***, the contribution of through-bond exchange interaction mechanism to the energy transfer process is negligible. For this reason Förster mechanism has been primarly considered. Within the frame of Förster theory, intra-EET as fast as those determined for ***f-Bi*** and ***r-Bi*** can be achieved only when Dn and Ac chromophores are at distances of 4–5 Å. In spite of the simplifications here adopted it is yet possible to evaluate the small structural differences existing among the two bichromophores. The conclusion is that the rigidity introduced by the pyrrolidine ring in ***r-Bi*** makes the Dn–Ac distance 10% larger than in ***f-Bi*** thus leading to a EET rate which is half of that measured in ***f-Bi***.

EET processes as fast as few ps have been already reported [39,46] even in the gas phase [52] and Förster theory successfully applied in the interpretation of the experimental data. However, it is worthwhile noticing that for $R_{Dn–Ac}$ as short as that estimated in the present work, a contribution of the short-range (Dexter) term to the intra-EET process cannot be excluded. For molecules at small distances, the through-space overlap of the electron clouds implies a penetration and electron exchange contributions to the rate constant [53]. Given the enhanced diffuseness of excited state wave functions, one would expect that at 5 Å short-range mechanisms can perturb the interchromophore interaction. The observed intra-EET in ***f-Bi*** is most likely not occurring by means of the purely Förster dipole–dipole interaction mechanism, but it may also involve a small contribution from the short-range interaction. The latter could be also responsible of the differences observed between the steady-state absorption spectra of the molecular Ac and of Ac in ***f-Bi*** and of the Ac fluorescence quantum yield enhancement in ***f-Bi***.

Acknowledgment

This work was supported by the Italian Ministero dell'Istruzione, dell'Universitàe della Ricerca (MIUR) and INSTM under the contract FIRB RBNE033KMA and by the European Community under the contract RIII-CT-2003-506350.

References

[1] G.D. Scholes, Annu. Rev. Phys. Chem. 54 (2003) 57.
[2] D. Gust, T.A. Moore, Adv. Photochem. 16 (1991) 1.
[3] J.P. Dekker, R. van Grondelle, Photosvnth. Res. 63 (2000) 195.
[4] B.A. Dinerl, F. Rappaport, Annu. Rev. Plant Biol. 53 (2002) 551.
[5] R. Huber, Angew. Chem. 101 (1989) 849.
[6] M. Du, X. Xie, Y. Jia, L. Mets, G.R. Fleming, Chem. Phys. Lett. 201 (1993) 535.
[7] R. Bonnett, Chemical Aspects of Photodynamic Therapy, Gordon & Breach, Canada, 2000.
[8] B.W. Henderson, T.J. Dougherty, J. Photochem. Photobiol. 55 (1992) 145.
[9] M.N. Berberan-Santos, P. Choppinet, A. Fedorov, L. Jullien, B. Valeur, J. Am. Chem. Soc. 122 (2000) 11876.
[10] M.N. Berberan-Santos, J. Canceill, J.C. Brochon, L. Jullien, J.M. Lehn, J. Pouget, P. Tauc, B. Valeur, J. Am. Chem. Soc. 114 (1992) 6427.
[11] P. Belser, A. von Zelewsky, M. Frank, C. Seel, F. Vögtle, L. DeCola, F. Barigelletti, V. Balzani, J. Am. Chem. Soc. 115 (1993) 4076.
[12] G. Denti, S. Campagna, S. Serroni, M. Ciano, V. Balzani, J. Am. Chem. Soc. 114 (1992) 2944.
[13] V. Balzani, F. Scandola, Supramolecular Photochemistry, Ellis Horwood, Chichester, 1991.
[14] V. Balzani, P. Ceroni, B. Ferrer, Pure Appl. Chem. 76 (2004) 1887.
[15] A.A. Lamola, N.J. Turro, Energy Transfer and Organic Chemistry, Benjamin, New York, 1961.
[16] S. Speiser, J. Photochem. 22 (1983) 195.
[17] S. Speiser, Chem. Rev. 96 (1996) 1953.
[18] G.W. Robinson, R.P. Frosch, J. Chem. Phys. 37 (1962) 1962.
[19] G.W. Robinson, R.P. Frosch, J. Chem. Phys. 38 (1963) 1187.
[20] S.H. Lin, J. Chem. Phys. 44 (1966) 3759.
[21] S.H. Lin, J. Chem. Phys. 58 (1973) 5760.
[22] M. Bixon, J. Jortner, J. Chem. Phys. 48 (1968) 715;
M. Bixon, J. Jortner, J. Chem. Phys. 50 (1969) 3284;
M. Bixon, J. Jortner, J. Chem. Phys. 50 (1969) 4061.
[23] G.D. Scholes, K.P. Ghiggino, J. Chem. Phys. 101 (1994) 1251.
[24] E.K.L. Yeow, D.J. Haines, K.P. Ghiggino, M.N. Paddon-Row, J. Phys. Chem. A 103 (1999) 6517.
[25] A. Aviram, M.M. Ratner (Eds.), Molecular Electronics: Science and Technology, vol. 852, New York Academy of Sciences, New York, 1998.
[26] F.L. Carter (Ed.), Molecular Electronic Devices, vol. II, Dekker, New York, 1987.
[27] Th. Förster, in: O. Sinanoglu (Ed.), Modern Quantum Chemistry, vol. 3, Academic Press, New York, 1965.
[28] A. Chattopadhyay, Chem. Phys. Lipids 53 (1990) 1.
[29] P.B. Ghosh, M.W. Whitehouse, Biochem. J. 108 (1968) 155.

[30] R.S. Fager, C.B. Kutina, E.W. Abrahamson, Anal. Biochem. 53 (1973) 290.
[31] S.J. Ferguson, W.J. Lloyd, G.K. Radda, Biochem. J. 159 (1976) 347.
[32] D. Evanko, Nature Meth. 2 (2005) 160.
[33] J.L. Adams, R.S. Garigipati, M. Sorenson, S.J. Schmidt, W.R. Brian, J.F. Newton, K.A. Tyrrel, E. Garver, L.A. Yodis, M. Chabot-Fletcher, M. Tzimas, E.F. Webb, J.J. Breton, E. Griswold, J. Med. Chem. 39 (1996) 5035.
[34] R. Ando, M. Kawamura, N. Chiba, J. Med. Chem. 44 (2001) 4468.
[35] W.H. Melhuish, J. Phys. Chem. 65 (1961) 229.
[36] D. Madge, R. Wong, P.G. Seybold, Photochem. Photobiol. 75 (2002) 327.
[37] F.V.R. Neuwhal, L. Bussotti, P. Foggi, Res. Adv. Photochem. Photobiol. 1 (2000) 77.
[38] P. Foggi, L. Bussotti, F.V.R. Neuwhal, Int. J. Photoenergy 3 (2001) 103.
[39] F.V.R. Neuwhal, R. Righini, A. Adronov, P.R.L. Malefant, J.M.J. Fréchet, J. Phys. Chem. B 105 (2001) 1307.
[40] A.D. Bacon, M.C. Zerner, Theo. Chim. Acta 53 (1979) 21.
[41] M.J.S. Dewar, E.G. Zoebisch, E.F. Healy, J.J.P. Stewart, J. Am. Chem. Soc. 107 (1985) 3902.
[42] Spartan, Wavefunction, Inc., Irvine, Ca, 2006.
[43] S. Saha, A. Samanta, J. Phys. Chem. A 102 (1998) 7903.
[44] D. Getz, A. Ron, M.B. Rubin, S. Speiser, J. Phys. Chem. 84 (1980) 768.
[45] S. Hassoon, H. Lustig, M.B. Rubin, S. Speiser, J. Phys. Chem. 88 (1984) 6367.
[46] J.A. Mondal, G. Ramakrishna, A.K. Singh, H.N. Ghosh, M. Mariappan, B.G. Maiya, T. Mukherjee, D.K. Palit, J. Phys. Chem. A 108 (2004) 7843.
[47] M.I. Ranasinghe, O.P. Varnaski, J. Pawlas, S.I. Hauck, J. Louie, J.F. Hartwig, T. Goodson, J. Am. Chem. Soc. 124 (2002) 6520.
[48] Y. Wang, M.I. Ranasinghe, T. Goodson, J. Am. Chem. Soc. 125 (2003) 9562.
[49] The molar extinction coefficients of Ac in f-Bi have been valuated by shifting the absorption spectrum of isolated Ac until it overlapped with that of f-Bi at the maximum of the S0 → S1 band.
[50] (a) T. Förster, Ann. Phys. 2 (1948) 55;
(b) T. Förster, Z.A. Naturforsh, Phys. Sci. 4 (1949) 321.
[51] B.W. Van der Meer, G. Coker III, S.Y. Simon Chen, Resonance Energy Transfer: Theory and Data, VCH Verlag, Weinheim, Germany, 1994.
[52] V.A. Povedailo, D.L. Yakoviev, J. Appl. Spect. 72 (2005) 495.
[53] G.D. Scholes, A.H.A. Clayton, K.P. Ghiggino, J. Chem. Phys. 10 (1992) 7405.